research papers

Understanding the highly efficient catalysis of prokaryotic peptide deformylases by shedding light on the determinants specifying the low activity of the human counterpart

Sonia Fieulaine,[a] Michel Desmadril,[b] Thierry Meinnel[a]* and Carmela Giglione[a]*

[a]CNRS, Centre de Recherche de Gif, Institut des Sciences du Végétal, Bâtiment 23A, 1 Avenue de la Terrasse, 91198 Gif-sur-Yvette CEDEX, France, and [b]Institut de Biochimie et Biophysique Moléculaire et Cellulaire, Université de Paris-Sud 11, Bâtiment 430, 91405 Orsay CEDEX, France

Correspondence e-mail: meinnel@isv.cnrs-gif.fr, giglione@isv.cnrs-gif.fr

Peptide deformylases (PDFs), which are essential and ubiquitous enzymes involved in the removal of the *N*-formyl group from nascent chains, are classified into four subtypes based on the structural and sequence similarity of specific conserved domains. All PDFs share a similar three-dimensional structure, are functionally interchangeable *in vivo* and display similar properties *in vitro*, indicating that their molecular mechanism has been conserved during evolution. The human mitochondrial PDF is the only exception as despite its conserved fold it reveals a unique substrate-binding pocket together with an unusual kinetic behaviour. Unlike human PDF, the closely related mitochondrial PDF1As from plants have catalytic efficiencies and enzymatic parameters that are similar to those of other classes of PDFs. Here, the aim was to identify the structural basis underlying the properties of human PDF compared with all other PDFs by focusing on plant mitochondrial PDF1A. The construction of a chimaera composed of plant PDF1A with the nonrandom substitutions found in a conserved motif of its human homologue converted it into an enzyme with properties similar to the human enzyme, indicating the crucial role of these positions. The crystal structure of this human-like plant PDF revealed that substitution of two residues leads to a reduction in the volume of the ligand-binding site together with the introduction of negative charges, unravelling the origin of the weak affinity of human PDF for its substrate. In addition, the substitution of the two residues of human PDF modifies the transition state of the reaction through alteration of the network of interactions between the catalytic residues and the substrate, leading to an overall reduced reaction rate.

1. Introduction

Peptide deformylases (PDFs) constitute a large subfamily of hydrolytic enzymes related to the thermolysin–metzincin HE*XX*H motif-containing family of metalloproteases (Boularot *et al.*, 2004; Schmitt *et al.*, 1996; Meinnel, 2000; Meinnel & Giglione, 2008). In the PDF subfamily a cysteine residue is involved in metal coordination within the active site, together with the above two histidines. PDFs are involved in the essential removal of the formyl group from the N-terminal methionine during the early phase of protein translation, barely after the nascent chain has emerged from the ribosome. Although the PDF enzyme was long believed to be a unique feature of bacteria, several studies have proved that PDF enzymes are found in almost all organisms, including not only prokaryotes and most eukaryotes but also viruses (Serero *et al.*, 2001; Dirk *et al.*, 2001, 2002; Giglione *et al.*, 2003; Ross *et al.*, 2005; Sharon *et al.*, 2011). Most of these orthologues display deformylase activity *in vivo* and/or *in vitro* (Giglione *et al.*,

2009). In eukaryotes, PDFs are expressed in the cytoplasm and targeted to plastids and/or mitochondria (Giglione *et al.*, 2000; Nguyen *et al.*, 2003; Serero *et al.*, 2003; Lee *et al.*, 2003).

Even though the different PDFs display low amino-acid sequence homology, the majority of these proteins exhibit an extremely strong conservation of the amino-acid residues in motifs 1–3 (motif 1, GΦGΦAAXQ; motif 2, EGCLS; motif 3, HEΦDHLXG; Φ is a hydrophobic amino acid and X is any amino acid; Boularot *et al.*, 2004). These motifs contain functionally important residues involved in metal coordination, substrate binding or catalysis (Becker, Schlichting, Kabsch, Groche *et al.*, 1998). The conservation of these motifs reflects the evolutionary importance of maintaining the essential catalytic activity of PDF enzymes. This is in line with the general assumption that proteins evolve by accepting many substitutions at residue positions that play little or no role in structure and function, while some amino acids cannot be changed by evolutionary processes without the risk of dramatically affecting the stability, the structure and/or the function of the protein (Bowie *et al.*, 1990). Hence, only the C-domain of PDF appears to be fully dispensable for activity (Meinnel *et al.*, 1996), with the rest of the protein being extremely compact and tightly folded.

Since its discovery, human mitochondrial PDF (*Hs*PDF) has drawn attention among the PDFs because of its unique unusual features, which however do not prevent the enzyme from displaying deformylase activity *in vivo* (Giglione *et al.*, 2000; Serero *et al.*, 2003). The crystal structure of *Hs*PDF solved alone or in complex with actinonin (a natural inhibitor of all PDF enzymes; Chen, Patel *et al.*, 2000; Van Aller *et al.*, 2005) showed a substrate-binding site specific to mitochondrial enzymes (Fieulaine *et al.*, 2005; Escobar-Alvarez *et al.*, 2009; Serero *et al.*, 2003). Despite having a conserved overall fold, *Hs*PDF displays nonrandom substitutions in two of the three conserved motifs (motifs 1 and 2) that build the active site. The first glycine in motif 1 is replaced by a cysteine (CVGLSAPQ) and the leucine in motif 2 is replaced by a glutamate (EGCES; Fig. 1*a*; Nguyen *et al.*, 2003; Serero *et al.*, 2003; Giglione *et al.*, 2000). Our previous studies have shown that these evolutionary substitutions are responsible for the unusual *in vitro* kinetic behaviour of *Hs*PDF, as the replacement of these two residues by those commonly found in other PDF enzymes (Cys to Gly and Glu to Leu) makes it act intermediately between *Escherichia coli* PDF (*Ec*PDF) and the mitochondrial PDF from the plant *Arabidopsis thaliana* (*At*PDF1A) (Serero *et al.*, 2003). Conversely, a single substitution of one of these two amino acids did not affect the atypical kinetics of *Hs*PDF, suggesting a functional link between these two residues. The reciprocal double substitution (*i.e.* Gly to Cys and Leu to Glu) in *At*PDF1A dramatically decreased the activity of the plant protein (Serero *et al.*, 2003). The same results w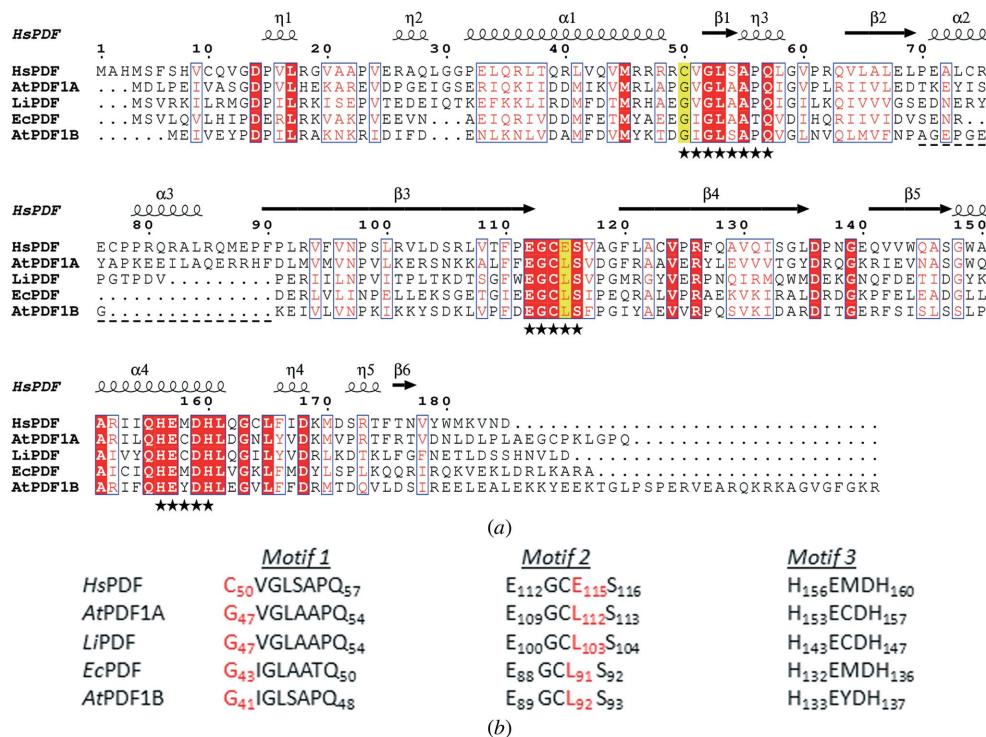ere obtained with a single mutation in *Ec*PDF (with Leu in motif 2 substituted by Ala) and with *Mycobacterium tuberculosis* PDF (Nguyen *et al.*, 2003; Narayanan *et al.*, 2011). Thus, the different behaviour of *Hs*PDF compared with other PDFs originates from its unique active site.

To investigate the evolutionary reasons for this specific unusual behaviour of *Hs*PDF and to obtain further insight into specific aspects of the conserved molecular mechanism underlying PDF enzymes, we studied the G47C/ L112E variant of *A. thaliana* mitochondrial PDF1A (see Fig. 1*b* for numbering of the *At*PDF1A enzyme), which perfectly mimics the wild-type (WT) human enzyme regarding structural and catalytic features (Fieulaine *et al.*, 2005). We conducted biochemical experiments with the resultant chimeric protein (defined as 'human-like' PDF) to characterize the effects of these mutations on stability and interactions with ligands. We have also solved the structure of this human-like PDF both alone and

Figure 1
Sequence alignment of several representative PDFs. (*a*) The sequence of mitochondrial PDF from *Homo sapiens* (*Hs*PDF; Escobar-Alvarez *et al.*, 2009) was aligned by *ESPript* (Gouet *et al.*, 1999) with *A. thaliana* PDF1A (*At*PDF1A), *Leptospira interrogans* PDF (*Li*PDF), *E. coli* PDF (*Ec*PDF) and *A. thaliana* PDF1B (*At*PDF1B). Black stars and the dashed line indicate the three conserved motifs and the CD-loop, respectively. The critical substitutions in the human sequence are highlighted in yellow. (*b*) Specific numbering of residues in the three conserved sequences of *Hs*PDF, *At*PDF1A, *Li*PDF, *Ec*PDF and *At*PDF1B. (PDB codes: *Hs*PDF, 3g5p; *At*PDF1A, 1zxz; *Li*PDF, 1y6h; *Ec*PDF, 1bs5; *At*PDF1B, 3m6o.)

Table 1
Crystallographic data and refinement statistics.

Values in parentheses are for the outer resolution shell.

Ligand	None	Actinonin	Met-Ala-Ser
Data			
Resolution (Å)	28.96–2.00	46.88–2.10	46.68–2.40
Space group	$P2_12_12_1$	$P2_12_12_1$	$P2_12_12_1$
Unit-cell parameters (Å)	$a = 51.45$,	$a = 51.84$,	$a = 51.55$,
	$b = 73.98$,	$b = 74.32$,	$b = 74.71$,
	$c = 109.39$	$c = 109.77$	$c = 109.76$
Measured intensities	136514	119178	135946
Unique reflections	28787	25011	32123
Completeness (%)	99.5 (99.4)	98.3 (98.4)	99.5 (97.2)
$\langle I/\sigma(I)\rangle$	19.53 (9.45)	10.59 (4.26)	11.68 (3.03)
R_{merge}† (%)	5.8 (13.7)	11.3 (34.7)	8.4 (38.6)
Refinement			
R_{work}/R_{free}‡ (%)	15.63/18.54	17.95/23.06	17.38/25.10
Mean B factor (Å^2)			
Chain A	12.2	22.0	45.6
Chain B	12.7	22.5	45.3
Ligand	—	29.7	42.9
R.m.s.d.			
Bonds (Å)	0.014	0.022	0.030
Angles (°)	1.354	1.990	2.667
Ramachandran plot, residues in (%)			
Most favoured regions	93.9	92.4	91.8
Additionally allowed regions	6.1	7.6	8.2
Generously allowed regions	0.0	0.0	0.0
Disallowed regions	0.0	0.0	0.0

† $R_{merge} = \sum_{hkl}\sum_i |I_i(hkl) - \langle I(hkl)\rangle|/\sum_{hkl}\sum_i I_i(hkl)$, where $I_i(hkl)$ is the intensity of a reflection and $\langle I(hkl)\rangle$ is the average intensity of that reflection. ‡ $R_{work} = \sum_{hkl} ||F_{obs}| - |F_{calc}||/\sum_{hkl} |F_{obs}|$. 5% of the data were set aside for R_{free} calculation.

in complex with the natural potent PDF inhibitor actinonin (Boularot *et al.*, 2007) or the tripeptide Met-Ala-Ser. Our results provide information to explain the drastic impact of only two substitutions on the activity of human mitochondrial peptide deformylase.

2. Materials and methods

2.1. Cloning, expression and purification

The recombinant human-like PDF protein, composed of 197 residues (Serero *et al.*, 2001) and carrying a C-terminal His$_6$ tag (the theoretical molecular mass of the monomeric protein is 22.3 kDa), was expressed and purified using nickel-affinity chromatography as described previously (Fieulaine *et al.*, 2005). The partially purified protein was then applied onto a Q Sepharose (GE Healthcare Life Sciences) anion-exchange column previously equilibrated in buffer *A* (50 m*M* HEPES pH 7.5). Elution was performed with a 20-column-volume gradient from 0 to 100% buffer *B* (50 m*M* HEPES pH 7.5, 1 *M* NaCl; Fourmy *et al.*, 1993; Schmitt *et al.*, 1993). Finally, the protein was applied onto a Superdex 75 column (GE Healthcare Life Sciences) and eluted at a constant flow rate (1.5 ml min^{-1}) in buffer *C* (50 m*M* HEPES pH 7.5, 100 m*M* NaCl). Human-like PDF-containing fractions were pooled, concentrated using an Amicon Ultra-15 centrifugal filter unit and stored at −80°C in buffer *C*. All purification procedures were performed at 4°C. The protein concentration was esti-mated from the calculated extinction coefficient at 280 nm (13 200 *M*$^{-1}$ cm^{-1}).

2.2. Size-exclusion chromatography

Gel-permeation experiments were performed on a Superdex 75 HR 10/30 column (GE Healthcare Life Sciences) equilibrated in buffer *C* and calibrated with molecular-mass markers (Blue Dextran 2000, ∼2000 kDa; bovine serum albumin, 67 kDa; ovalbumin, 43 kDa; chymotrypsinogen A, 25 kDa; ribonuclease A, 13.7 kDa; GE Healthcare Life Sciences). Samples with a protein concentration of 2 mg ml^{-1} were centrifuged (10 min, 14 000 rev min^{-1} at 4°C) and 100 µl was loaded onto the column. Elution was performed in buffer *C* at a constant flow rate (0.5 ml min^{-1}). The area of each peak integrated using the *Unicorn* software allowed us to estimate the quantity of monomers, dimers and trimers.

2.3. Microcalorimetry

ITC and DSC experiments were performed as described previously (Fieulaine *et al.*, 2011) with several modifications as reported below. ITC experiments were performed at 25°C. Ligands (actinonin and Met-Ala-Ser) and proteins (*At*PDF1A and human-like PDF) were dissolved in buffer *C*. The proteins were centrifuged before the experiments and the concentra-tion of the soluble fraction was determined by measurement of the absorbance at 280 nm. The protein concentration in the microcalorimeter cell varied from 10 to 30 µ*M*. A total of 25 injections of 10 µl of ligand solution at concentrations varying from 150 to 450 µ*M* were added at intervals of 240 s while stirring at 310 rev min^{-1}. For each measurement, the heat of dilution of the ligand was subtracted from the protein titration before fitting the data, providing a zero value of ΔH at saturation. The heat of dilution was evaluated using either direct blank titration of the ligand into the buffer or the heat measured after saturation. The two analyses gave the same result. The experimental data were fitted to a theoretical titration curve using the *Origin* software (MicroCal) with ΔH (the enthalpy change), K_a (the association binding constant in M^{-1}) and n (the number of binding sites per monomer) as adjustable parameters and the total protein concentration and the free and total ligand concentrations as known parameters.

DSC experiments were performed with proteins (22 µ*M* *At*PDF1A or human-like PDF) in the absence or the presence of ligand (67 µ*M* actinonin or Met-Ala-Ser). Each measure-ment was preceded by a baseline scan with buffer *C*. The ITC and DSC experiments were repeated twice. When the data were noisy (*i.e.* in ITC experiments with the MAS peptide) the experiments were replicated three or four times.

2.4. Crystallization and structure determination

The crystallization condition used for human-like PDF was the same as that used for wild-type *At*PDF1A (Fieulaine *et al.*, 2005). PEG 5000 MME or PEG 6000 was employed as a precipitant. The structure of the human-like PDF–Met-Ala-Ser complex was obtained from crystals soaked with 10 m*M* Met-Ala-Ser, whereas the structure of the human-like PDF–actinonin complex was obtained by co-crystallization with 15 m*M* actinonin. Crystals were transferred into a solution composed of 15% PEG 5000 MME or PEG 6000, 100 m*M*

MES buffer pH 5.5, 20% glycerol and flash-cooled in liquid nitrogen using cryoloops. Data collection was performed at 100 K on stations FIP-BM30A and ID14-eh2 at the European Synchrotron Radiation Facility, Grenoble, France. Data were processed and scaled with *XDS* (Kabsch, 2010; Table 1).

The structure of free human-like PDF was solved by molecular replacement with *Phaser* (McCoy *et al.*, 2005) followed by rigid-body refinement with *CNS* (Brünger *et al.*, 1998) using the coordinates of wild-type *At*PDF1A as a search model (PDB entry 1zxz; Fieulaine *et al.*, 2005). The structures of ligand-bound proteins were solved by rigid-body refine-

ment in *CNS* using the free human-like PDF structure. The three final models were obtained by manual rebuilding using *TURBO-FRODO* (Roussel & Cambillau, 1989) combined with refinement using only calculated phases with *CNS* and *REFMAC* (Murshudov *et al.*, 2011). Quality control of the models was performed with *PROCHECK* (Laskowski *et al.*, 1993). The statistics for the three final refined models are given in Table 1. The presence of anomalous ions was investigated by X-ray fluorescence experiments. One crystal of free human-like PDF was mounted on the goniometer head and exposed to the X-ray beam, and the fluorescence emitted by the crystal was monitored by a multi-channel fluorescence detector (Röntec, Germany).

The coordinates and structure factors have been deposited in the RCSB Protein Data Bank with accession codes 4je6, 4je7 and 4je8. Figures were generated using *PyMOL* (DeLano, 2002).

3. Results

3.1. Construction of human-like peptide deformylase and analysis of its stability and affinity for ligands

All animal PDFs are characterized by two identical substitutions in two of the three conserved motifs which characterize the PDF enzyme family (see Fig. 1 of Serero *et al.*, 2003 and §1). Since these substitutions do not occur in the highly active and stable *A. thaliana* mitochondrial peptide deformylase *At*PDF1A (Fig. 1) and site-directed mutagenesis of these residues in *Hs*PDF was sufficient to render it indistinguishable from *At*PDF1A (Serero *et al.*, 2003), it was hypothesized that these evolutionary amino-acid substitutions contribute to determining the unusual features of human peptide deformylase. In order to verify this hypothesis, we decided to produce a human-like peptide deformylase corresponding to the mitochondrial PDF from *A. thaliana* carrying the double substitution G47C/L112E which mimics the modified active site of the human PDF. Similar to the genuine *At*PDF1A and *Hs*PDF (Fieulaine *et al.*, 2005; Escobar-Alvarez *et al.*, 2009), the purified human-like peptide deformylase was found to behave mainly as a dimer in solution, with an experimental molecular mass of 46.1 kDa (Fig. 2*a*). A minor amount of
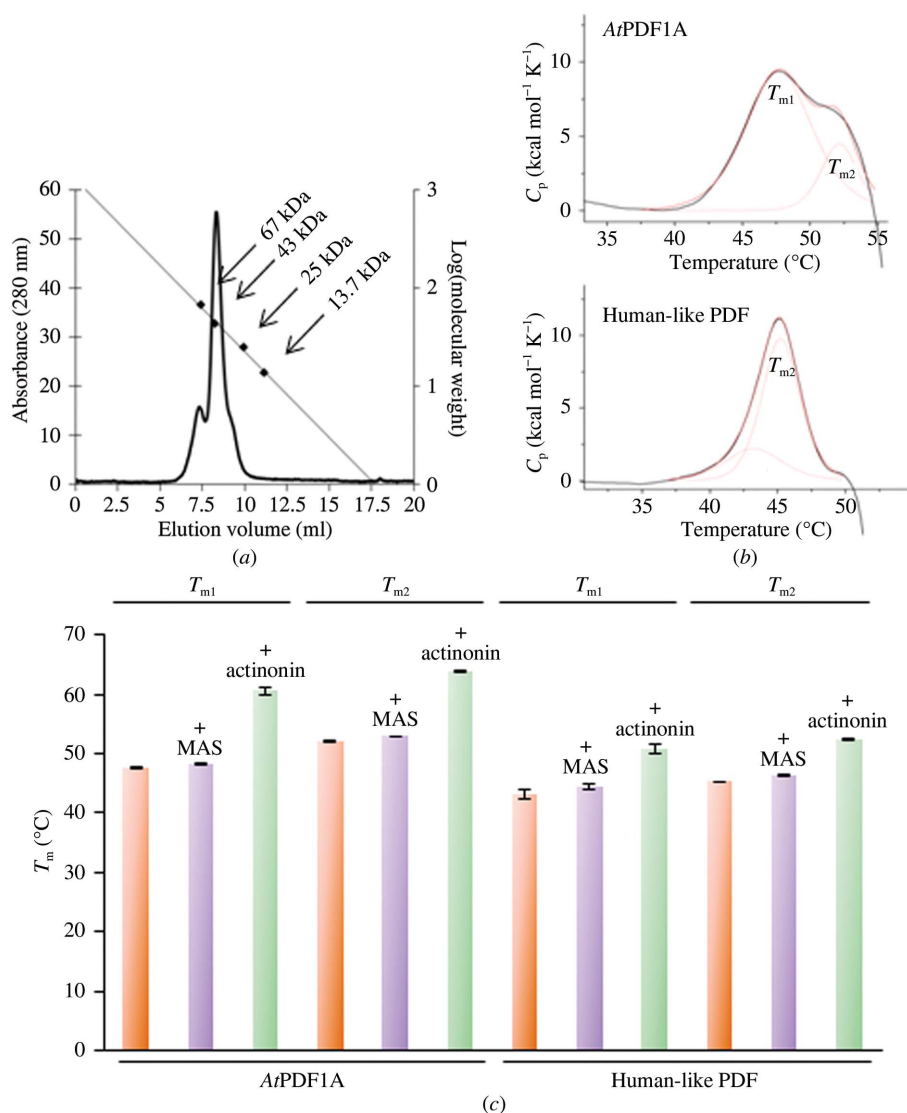
Figure 2
The evolutionary double substitution G47C/L112E found in human PDF strongly disturbs the stability of the protein. (*a*) Size-exclusion chromatographic analysis of human-like PDF. The elution profile on Superdex 75 is shown, as well as the calibration plot obtained by column calibration with standard globular proteins ranging in size from 13.7 to 67 kDa. (*b*) Denaturation of wild-type and human-like *At*PDF1A. Raw data (solid black line) of thermograms for *At*PDF1A (top) and human-like PDF (bottom) are superposed on the best fit (solid red line) composed of two peaks (red dotted lines). DSC thermograms are baseline-corrected. (*c*) Apparent transition temperature (T_m) in several experimental conditions. For each protein (*At*PDF1A and human-like PDF), T_m values for the two transition peaks are given corresponding to three distinct experiments: free enzyme and Met-Ala-Ser (MAS) or actinonin-bound enzyme (orange, purple and green bars, respectively). Standard errors are indicated for each point (a maximum standard error of 0.8°C was observed).
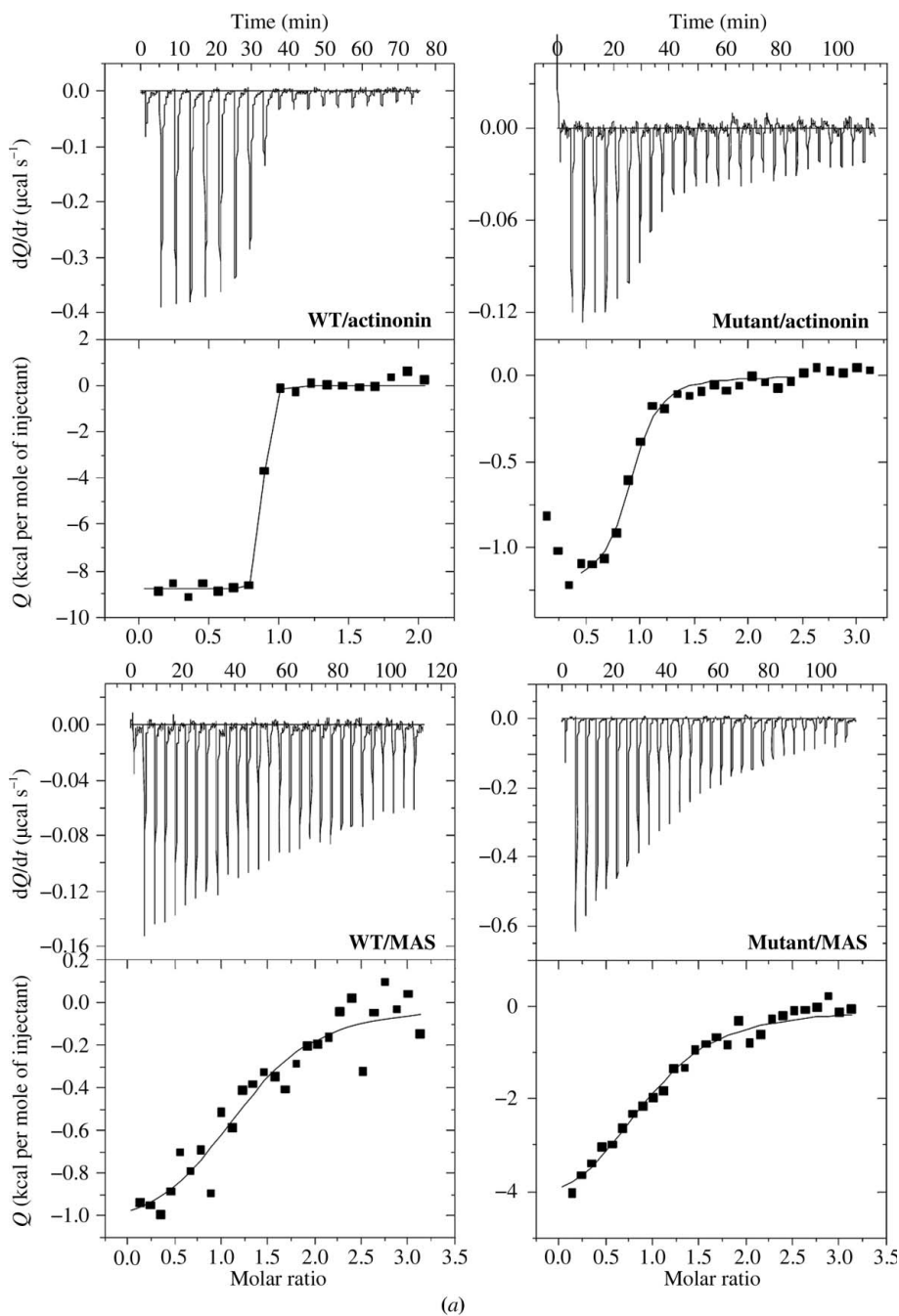
monomer and trimer was also found in the enzyme preparation, representing approximately 10 and 18%, respectively.

In order to evaluate the roles of these evolutionary substitutions in protein stability, the thermal denaturation of both wild-type (WT) *At*PDF1A and human-like PDF was measured using differential scanning calorimetry (DSC) experiments. The DSC curves were fitted with both one and two transitions. Clearly, the melting curves cannot be fitted using a single transition: the residual values were not homogeneously centred on zero mean, showing a significant lack of fit. Using two transitions, the residual values were homogeneously centred on zero mean and the χ_2 value was clearly improved, with the value being reduced by a factor of 100. Indeed, as shown in Fig. 2(*b*), the transition between folded and unfolded states is asymmetric and can be dissociated into two events which may correspond to (i) dissociation of the dimer followed by monomer denaturation or (ii) an event most likely related to the heterogeneity of the enzyme preparation (Fig. 2*a*). Unfortunately, owing to the repeatable precipitation of both proteins at temperatures higher than 50–55°C, complete analysis of the thermograms was not possible. It is nevertheless clear that the change in the excess heat capacity (C_p) was higher for the first denaturation event compared with the second event in the case of *At*PDF1A, whereas the situation was the opposite for the human-like PDF. It was also possible to estimate the apparent transition temperature (T_m) for each denaturation event with good confidence (Fig. 2*c*), which was slightly lower in the case of human-like PDF (a difference of ∼6°C). These results indicated that the G47C/L112E double substitution renders *At*PDF1A less stable than the WT form. Moreover, these values clearly show that the presence of the tripeptide Met-Ala-Ser does not change the unfolding process of both proteins ($\Delta T_{m1} = \Delta T_{m2} = 1$°C), whereas actinonin, the natural inhibitor of PDF enzymes (Chen, Patel *et al.*, 2000; Van Aller *et al.*, 2005), systematically stabilizes both variants by increasing the temperature of

Figure 3
The two mutations of human PDF decrease the affinity for ligands. (*a*) ITC data. Wild-type (WT) or human-like (mutant) PDF were titrated with actinonin or the tripeptide Met-Ala-Ser (MAS). The top panels represent raw data, whereas the bottom panels correspond to the fit of the titration curves. (*b*) Tabular view of the results showing the dissociation constant (K_d) and the stoichiometry derived from the fitting of the experimental data. The double mutation G47C/L112E in *At*PDF1A mimics the modified active site of *Hs*PDF.

denaturation, $\Delta T_{m1} \simeq \Delta T_{m2} \simeq 15°C$ for AtPDF1A and $\Delta T_{m1} \simeq \Delta T_{m2} \simeq 9°C$ for human-like peptide deformylase, as previously reported for bacterial PDF (Fieulaine *et al.*, 2011).

The effect of the G47C and L112E mutations on the affinity for Met-Ala-Ser and actinonin was further investigated using isothermal titration calorimetry (ITC). As previously shown for bacterial PDF (Van Aller *et al.*, 2005; Berg & Srivastava,

2009; Amero *et al.*, 2009; Fieulaine *et al.*, 2011), our ITC titration curves were consistent with a very strong affinity of actinonin for both WT and human-like AtPDF1A, enabling us to determine an accurate dissociation constant (K_d; Fig. 3). Actinonin showed an affinity for AtPDF1A in the nanomolar range, in agreement with the values generated by other means for various PDFs (Chen, Choi *et al.*, 2000; Boularot *et al.*, 2007; Berg & Srivastava, 2009; Amero *et al.*, 2009; Serero *et al.*, 2003; Fieulaine *et al.*, 2011). This affinity was significantly decreased for the human-like peptide deformylase (by two orders of magnitude). Similarly, but to a lesser extent, the affinity of the tripeptide Met-Ala-Ser was lower for human-like peptide deformylase compared with AtPDF1A. This indicates the importance of the residues at both positions 47 and 112 in modulating the affinity
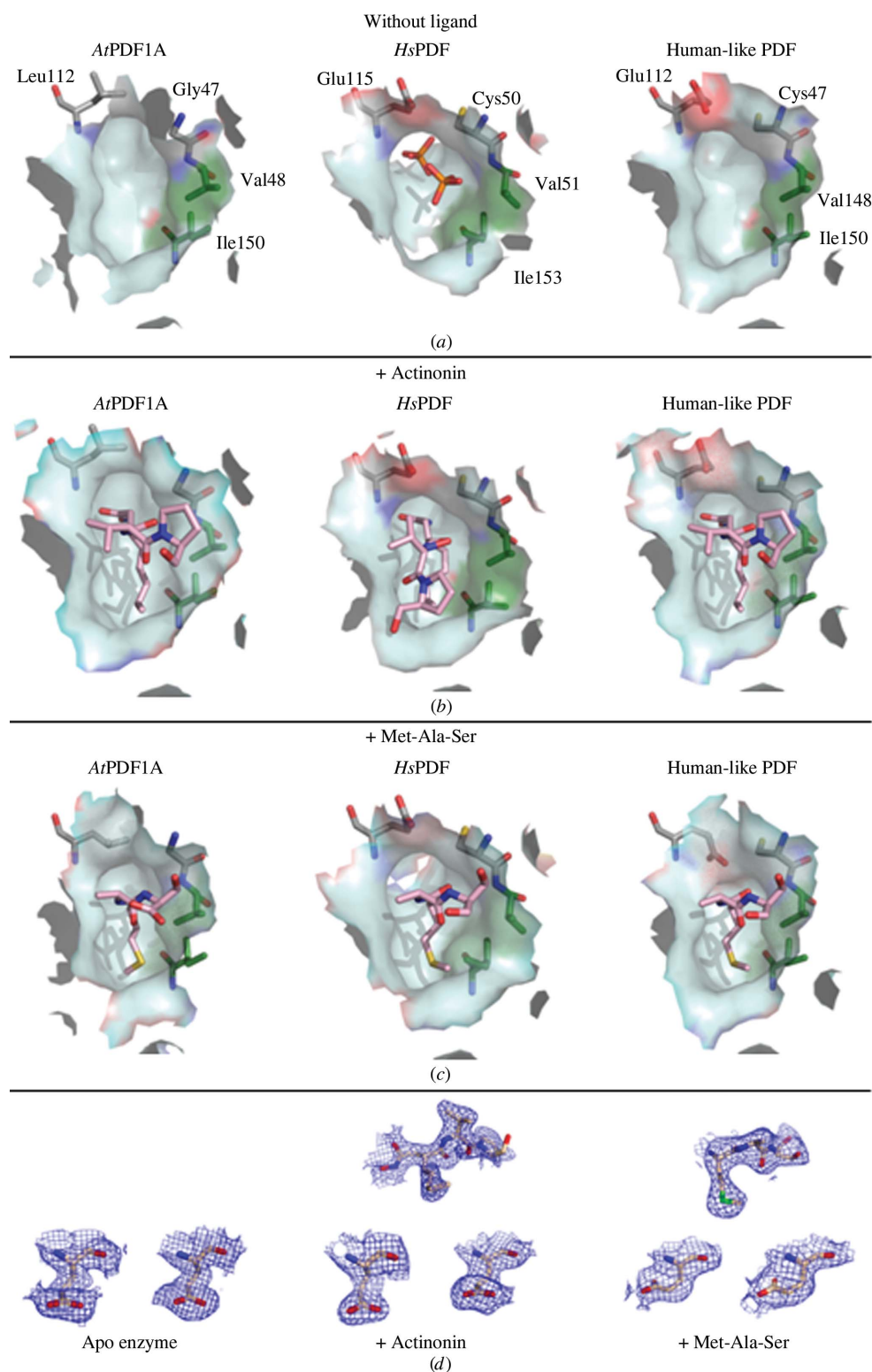

Figure 4
The conformation of the S1′ pocket in AtPDF1A, HsPDF and human-like PDF is shown. The solvent-accessible surface of the S1′ pocket is represented. The two residues that are studied in this work are represented, *i.e.* Gly47 or Cys47 and Leu112 or Glu112 for *A. thaliana* PDF, and Cys50 and Glu115 for HsPDF. Two residues (Val and Ile) among those which constitute the S1′ pocket are also represented and are coloured green. O, N, S and P atoms are coloured red, blue, yellow and orange, respectively. (*a*) Free AtPDF1A, HsPDF and human-like PDF. Two inorganic phosphate ions are present in the active site of HsPDF. (*b*) PDFs in complex with actinonin. (*c*) PDFs in complex with Met-Ala-Ser. (*d*) Ligands and the side chain of Glu112 in the three human-like PDF structures are drawn in stick representation and are shown as $F_o - F_c$ electron-density OMIT maps contoured at 2σ. For each structure the conformation of the Glu112 side chain is shown for both subunits *A* and *B* in the asymmetric unit (left and right, respectively). The structures used for this figure are PDB entries 1zxz, 1zy1 (Fieulaine *et al.*, 2011), 3g5p and 3g5k (Escobar-Alvarez *et al.*, 2009) and structures from this work for human-like PDF. Models of the AtPDF1A–actinonin and HsPDF–Met-Ala-Ser complexes were made as no experimental structures are available. Superimpositions between moving (human-like PDF–ligand complexes) and fixed (wild-type AtPDF1A or HsPDF) structures were performed using *SUPERPOSE* in the *CCP*4 package with the secondary-structure matching tool.

of the ligand for PDF. Moreover, fitting of the experimental data did not correspond to a 1:1 stoichiometry between enzyme and ligand (Fig. 3b), probably because the protein preparation did not contain only dimeric enzyme but also monomers and trimers (Fig. 2a).

3.2. Cys47 and Glu112 contribute alone to create a narrow active site in *At*PDF1A resembling that of *Hs*PDF

Despite a contrasting deformylase activity and a very low sequence identity between *At*PDF1A and *Hs*PDF (35%; Fig. 1), the solution of the corresponding crystal structures highlighted that the two enzymes display a conserved overall fold with a substrate-binding site specific to the mitochondrial enzymes, especially the presence of a long CD-loop (Fieulaine et al., 2005; Escobar-Alvarez et al., 2009). *At*PDF1A behaves as a dimer, with the C-terminal residues lying at the interface between the two subunits (Fieulaine et al., 2005). This arrangement is similar to that of *Leptospira interrogans* PDF, the only other dimeric bacterial PDF identified to date (Zhou et al., 2005). WT mitochondrial *At*PDF displayed an S1' pocket (i.e. the pocket into which the side chain of the N-terminal methionine fits) composed not only of residues Val48, Glu109, Trp146, Arg149, Ile150 and His153 (Fieulaine et al., 2005) but also of residues Gly47 and Leu112 (Fig. 4a), the two residues which were substituted in human PDF (Fig. 1). Several

features, including the fact that the side chains of both mutated residues face the opening of the active-site cavity (Fig. 4a), were considered as being responsible for the particular shape of the *Hs*PDF active-site entrance, characterized by a narrower atrium compared with bacterial PDFs (Serero et al., 2003; Fieulaine et al., 2005).

The human-like PDF was crystallized under the same conditions as wild-type *At*PDF1A and gave equivalent crystals with two identical molecules in the asymmetric unit corresponding to a biological homodimer. The overall structure of the protein closely mirrored that of WT *At*PDF1A (Fieulaine et al., 2005) and by extension the structure of *Hs*PDF, with the average root-mean-squared deviation being less than 0.4 Å for 100% of the C^α positions. X-ray fluorescence studies showed that the metal cation present within the active site was zinc. The protein was expressed without the addition of any metal and the crystallization buffer did not contain any metal, which means that human-like PDF naturally binds zinc ion, as was previously shown for wild-type *At*PDF1A (Serero et al., 2001; Fieulaine et al., 2005). Since human PDF contains cobalt within the crystal (Escobar-Alvarez et al., 2009) and probably iron in solution (Serero et al., 2003), this observation indicates that the double substitution is not involved in metal recruitment. Finally, no significant alteration of side-chain positions was observed between WT *At*PDF1A and the human-like PDF. Nevertheless, only the double substitutions G47C and
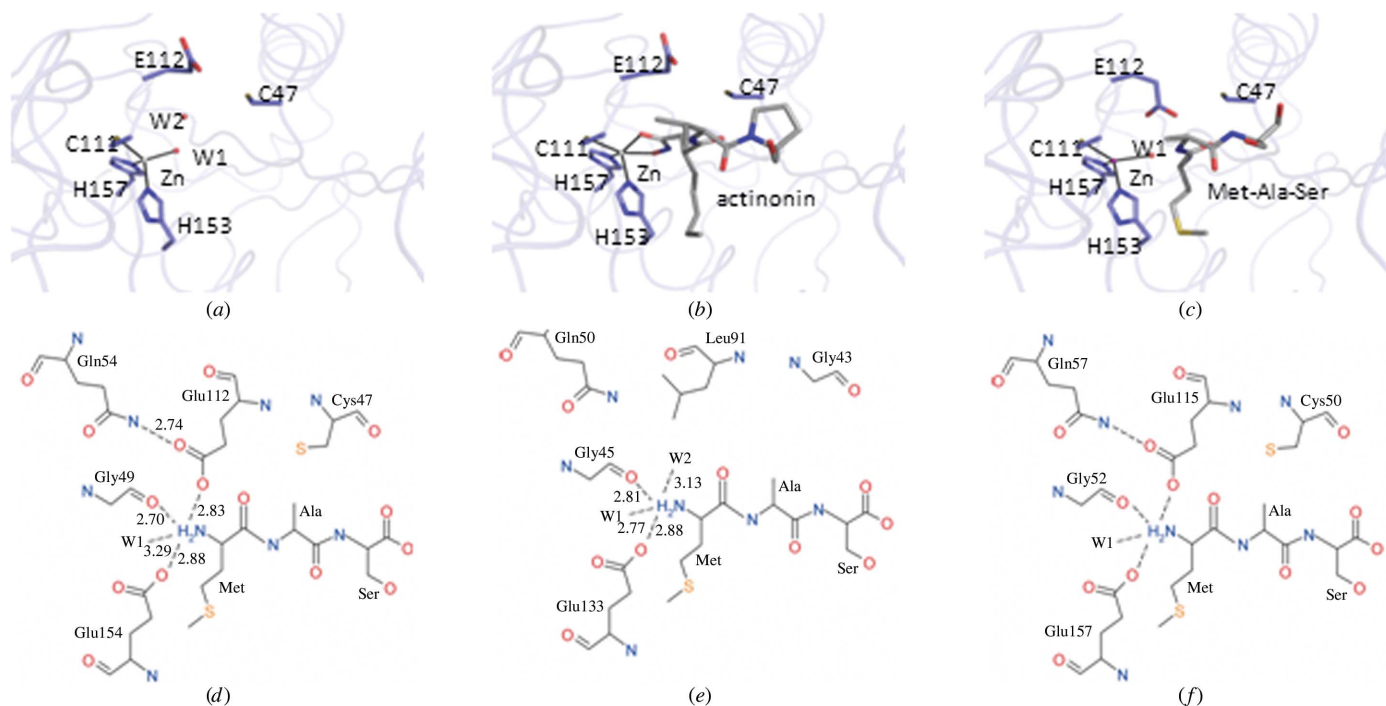

Figure 5
The leucine-to-glutamate mutation in motif 2 of human PDF strongly modifies the network of interactions in the oxyanion hole-like state during the deformylation reaction. Top row: the coordination shell of the catalytic metal in human-like PDF. Some side chains of the active site and the ligands are shown in stick format, with O atoms in red, N atoms in blue and S atoms in yellow. Water molecules W1 and W2 which are implicated in the enzymatic reaction (Becker, Schlichting, Kabsch, Groche et al., 1998) are also represented. The zinc ion identified within the active site is shown as a purple sphere. Solid lines indicate the coordination bonds of the zinc ion. (a) Empty human-like PDF. (b) Human-like PDF in complex with actinonin. (c) Human-like PDF in complex with Met-Ala-Ser. Bottom row: binding mode of Met-Ala-Ser in the active site of mitochondrial PDF. The network of interactions around the N-terminal amino group of Met-Ala-Ser in several PDF enzymes is represented. Dotted lines represent the hydrogen bonds, with lengths indicated in Å. (d) Human-like PDF (this work). (e) *Ec*PDF (PDB entry 1bs6). (f) *Hs*PDF (the complex is modelled; see Fig. 4).

L112E changed the nature of the S1′ pocket of human-like PDF, making the entrance to the active site narrower and more similar to that of *Hs*PDF (Fig. 4*a*).

3.3. Structure of human-like PDF in complex with the transition-state analogue actinonin or the natural product Met-Ala-Ser

Co-crystallization experiments with human-like PDF crystals allowed us to obtain a complex with the transition-state analogue actinonin, a pseudotripeptide hydroxamate derivative known to be one of the most potent PDF inhibitors. The overall structure of human-like PDF was not modified by actinonin (average root-mean-square deviation of 0.2 Å for 100% of the C$^\alpha$ positions). Nevertheless, the binding of actinonin to the human-like PDF changed the coordination shell of the catalytic cation (Figs. 5*a* and 5*b*), as was initially observed with bacterial PDFs (Clements *et al.*, 2001). Unlike the human-like PDF, it has been shown that the binding of actinonin induces a conformational change in several PDF enzymes of type 1B (Fieulaine *et al.*, 2011; Zhou *et al.*, 2005),

Figure 6
Evolutionary conservation of residues in the PDF family. Estimation of the evolutionary conservation of amino-acid positions in PDF family members was achieved with *ConSurf* 2010 (Landau *et al.*, 2005; Ashkenazy *et al.*, 2010). The search for homologous sequences of the most representative member of the PDF family, *i.e. Ec*PDF (PDB entry 1bs5), was performed using *PSI-BLAST* against the UniRef90 sequence databank using default parameters. The continuous conservation scores are divided into a discrete scale of nine grades for visualization: from the most variable positions (grade 1) coloured turquoise, through intermediately conserved positions (grade 5) coloured white, to the most conserved positions (grade 9) coloured maroon. These conservation scores are projected onto the *Ec*PDF structure viewed towards the catalytic site.

resulting in a closure of the active site to strongly increase the affinity. In human PDF, binding of actinonin led to a small induced-fit effect (Fig. 4*b*; Escobar-Alvarez *et al.*, 2009), with local structural rearrangement of the Val51 and Ile153 side chains, optimizing the hydrophobic contacts between the aliphatic chain of actinonin and the S1′ pocket. None of these effects was observed after the binding of actinonin in the human-like PDF active site (Fig. 4*a* and 4*b*).

The crystal structure of human-like PDF in complex with a natural PDF reaction product, Met-Ala-Ser, has been also solved. In contrast to actinonin, the binding of Met-Ala-Ser within the active site of human-like PDF was accompanied by a flip of the Glu112 side chain towards the peptide (Figs. 4*a*, 4*c*, 5*a* and 5*c*), resulting in two strong modifications. Firstly, in the final complex (Fig. 5*d*) the N-terminal amino group of the peptide formed several hydrogen bonds to Gly49 from motif 1, Glu154 from motif 3 and a water molecule (W1) as previously described for *E. coli* PDF (Becker, Schlichting, Kabsch, Groche *et al.*, 1998; Fig. 5*e*). In addition, a new hydrogen bond was observed to the side chain of Glu112 (Fig. 5*d*), which in turn also established a hydrogen bond to the Gln54 (motif 1) side chain. Secondly, the flip of Glu112 towards the tripeptide evicted the water molecule W2 (Figs. 5*a*, 5*c*, 5*d* and 5*e*), which is commonly hydrogen bonded to the N-terminal amino group of the peptide in enzyme–product complexes of bacterial PDFs (Becker, Schlichting, Kabsch, Groche *et al.*, 1998; Fig. 5*e*). Finally, we proceeded to a soaking experiment in which a substrate of the reaction, the formylated tripeptide Fo-Met-Ala-Ser, was added to the crystals. Since the deformylation reaction occurred within the crystal, as has been shown for other PDFs (Fieulaine *et al.*, 2011), we could solve the structure of the human-like PDF–Met-Ala-Ser complex corresponding to a true enzymatic conformation at the end of the deformylation reaction. In this case, the final complex and the interactions between the enzyme and the product were fully similar to those described above.
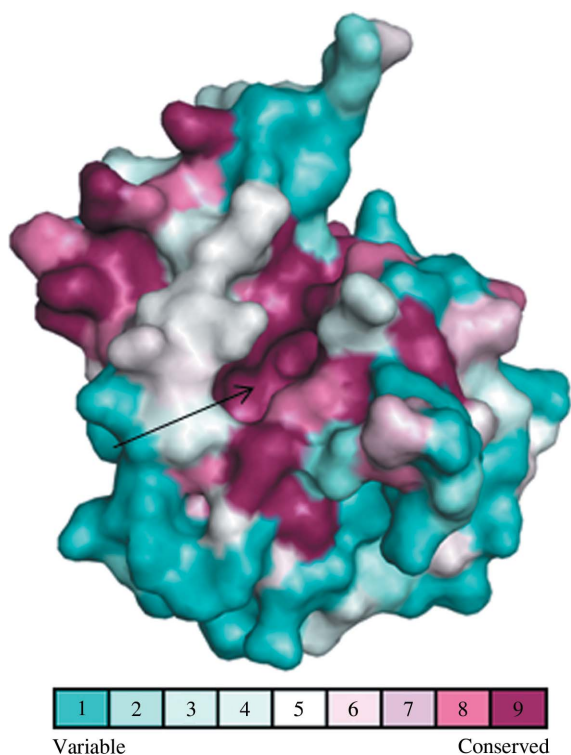
4. Discussion

As for the genetic code, the amino-acid sequence code is highly degenerate. Indeed, different sequences can induce folding into the same three-dimensional structure and finally give the same enzymatic function. In this degeneration of the amino-acid sequence code, some amino acids cannot be changed by evolutionary processes as this would dramatically affect the stability, the structure and/or the function of the protein. Mostly, these residues are conserved through evolution. In this context, peptide deformylases (PDFs) are a good example of a large protein family with a fold and an activity that are highly conserved through kingdoms and cellular compartments despite a low overall amino-acid sequence similarity (~35%). However, it is easy to highlight three conserved motifs among all PDFs (see §1 for more details) for which the importance of key residues for ligand binding and catalysis is reflected by a strong evolutionary pressure to resist amino-acid replacements in the active site (Fig. 6). Indeed, these residues are under strong selection and have been shown

many times to not accept any substitutions (Meinnel *et al.*, 1995, 1997; Ragusa *et al.*, 1999; Dardel *et al.*, 1998). Nonetheless, the idiosyncratic mammal mitochondrial PDFs, including the human enzyme, are the only exception to this constraint, systematically displaying two major mutations in two of the three conserved motifs (Serero *et al.*, 2003).

A number of independent data have revealed that *Hs*PDF is catalytically active but displays significantly weak activity (Nguyen *et al.*, 2003; Serero *et al.*, 2003; Lee *et al.*, 2003, 2004; Escobar-Alvarez *et al.*, 2009). Despite this low activity, its three-dimensional structure is similar to those of other PDFs (Escobar-Alvarez *et al.*, 2009). As this similarity encompasses the active site and the ligand-binding site, this implies that *Hs*PDF deformylates its substrates according to the enzymatic mechanism scheme described for bacterial PDF (Becker, Schlichting, Kabsch, Groche *et al.*, 1998). However, it has been proposed that the two major evolutionary substitutions (Fig. 1) are responsible for the significantly lower catalytic activity of *Hs*PDF (Serero *et al.*, 2003; Nguyen *et al.*, 2003). Despite many studies, the molecular details allowing the determination of the precise effects of these mutations have not yet been elucidated. With the use of a human-like enzyme consisting of *A. thaliana* mitochondrial PDF carrying the two mutations G47C/L112E (Serero *et al.*, 2003), we now provide biochemical and structural evidence strongly suggesting that these two mutations are responsible for (i) the decreased affinity for the substrate, (ii) the slower turnover of the enzyme and (iii) the reduced overall stability.

PDF enzymes usually behave as monomeric proteins, with only a couple of multimeric forms having been reported. Mitochondrial PDF1A from *A. thaliana* (*At*PDF1A) and bacterial PDF from *L. interrogans* are two well documented dimeric PDFs (Li *et al.*, 2002; Zhou *et al.*, 2004; Fieulaine *et al.*, 2005). It has been proposed that human PDF is also dimeric (Escobar-Alvarez *et al.*, 2009). The biological significance of a dimeric state for these PDFs remains unclear. In this work, we show that the double G47C/L112E substitution does not alter the oligomeric state of the human-like PDF in solution and in the crystalline state (Fig. 2). In contrast, we reveal that the double substitution G47C/L112E is linked to the thermal stability of the protein (Figs. 2*b* and 2*c*). Accordingly, it has previously been shown that the human enzyme is prone to degradation, precipitation and aggregation (Nguyen *et al.*, 2003; Serero *et al.*, 2003; Lee *et al.*, 2003).

The presence of a cysteine residue instead of the first glycine in motif 1 together with the substitution of the leucine by a glutamate in motif 2 (Fig. 1) appears to affect the optimal binding of the substrate within the active site. Indeed, we show in this work that the side chain of this cysteine decreases the volume of the S1' pocket by lowering its ceiling (Fig. 4), while the glutamate side chain, which brings a negative charge, alters the hydrophobicity of the S1' pocket. The impact of these structural modifications in the S1' pocket owing to the double substitution in the active site has been quantified by microcalorimetry experiments. In this context, we have shown that compared with WT *At*PDF1A the dissociation constant of human-like PDF was strongly decreased for actinonin and the

Table 2
Effect of mutations on the kinetic parameters of human PDF and *A. thaliana* PDF1A as reported in Serero *et al.* (2003) but taking into account the specific sequence numbering of human and *A. thaliana* PDF used in this study.

	K_m (mM)	k_{cat} (s^{-1})
Human PDF		
Wild type	1.6 ± 0.4	0.03 ± 0.005
C50G	nd†	nd
E115L	2.6 ± 0.6	0.07 ± 0.01
C50G/E115L	0.9 ± 0.2	2.1 ± 0.3
A. thaliana PDF1A		
Wild type	0.25 ± 0.07	22 ± 2
G47C	0.25 ± 0.08	0.19 ± 0.03
L112E	1.60 ± 0.60	0.023 ± 0.003
G47C/L112E	0.70 ± 0.20	0.11 ± 0.02

† Not determined.

reaction product Met-Ala-Ser (Fig. 3). In the case of Met-Ala-Ser, it is not surprising that the affinity is weaker than that of actinonin in the absence of any substitution as it represents the product of the deformylation reaction, which has to dissociate from the enzyme to allow the free enzyme to start a new catalytic cycle with a new substrate. In contrast to actinonin, the role of Met-Ala-Ser is therefore to promote the dissociation of the complex instead of its stabilization. Taken together, these results are consistent with the fact that the G47C/L112E double mutation in mitochondrial PDF1A from *A. thaliana* decreases the Michaelis constant for the substrate (Table 2). In contrast, *Hs*PDF with the reverse double mutation (C50G/E115L) exhibits a better affinity for the ligand than the wild-type enzyme (Table 2).

A detailed mechanism for the deformylation of an *N*-formylated methionine of a newly synthesized protein catalyzed by peptide deformylase has been described (Becker, Schlichting, Kabsch, Schultz *et al.*, 1998). According to this mechanism (see Fig. 3 of Becker, Schlichting, Kabsch, Groche *et al.*, 1998), the formylated substrate binds to the active site, with the carbonyl O atom of the formyl group replacing the water molecule W2 and being polarized by hydrogen bonds to the amide of Leu91 in motif 2 and the side chain of Gln50 in motif 1 (numbering of the *E. coli* enzyme; equivalent to L112E and Gln54, respectively, in human-like PDF1A; Fig. 1). This network of interactions is propitious to nucleophilic attack on the carbonyl C atom of the formyl group by the water molecule W1 (Figs. 5*d*, 5*e* and 5*f*). This leads to a transition state which is oxyanion hole-like, in which the carbonyl O atom of the formyl group is tetrahedrally ligated by the catalytic metal, the carbonyl C atom, the side-chain amide of Gln50 and the main-chain amide of Leu91. The side chain of Glu133 (Glu154 in human-like PDF) from motif 3 is then implicated in the transfer of the W1 proton to the N-terminal amide of the peptide, the added positive charge making the N atom suitable as a leaving group. Subsequent bond cleavage leads to a ternary enzyme–formate–peptide complex, followed by the dissociation of the complex. Thus, three residues play a critical role in the deformylase enzymatic mechanism: a conserved Gln from motif 1, the Leu from motif 2, both of which stabilize the transition state by forming an oxynanion-like hole, and the

Glu of motif 3, which aids the transfer of a proton from water molecule W1 to the peptide. Despite extensive study of this mechanism, how the PDF enzyme achieves the catalytically competent state remained elusive for a long time. Recently, using *At*PDF1B we provided insight into how PDF enzymes might reach this catalytically competent conformation by moving specific reactive groups into proximity to promote efficient deformylation (Fieulaine *et al.*, 2011). Accordingly, it is now suggested that free PDFs might exist in at least two conformational states (open or super-closed) and that the relative abundance of each conformation depends on each PDF form. In the particular case of *At*PDF1B, we have shown that the most abundant form of the free enzyme is probably the open state and that the binding of the ligand to the enzyme induces a structural transition at the active site that transforms the enzyme from the open to a closed enzymatically productive conformation. Between the open and the closed states, a hydrophobic pocket rearrangement mediated by structural changes of the side chains of Ile42, Phe58 and Ile130 (corresponding to Val48, Leu64 and Ile150 in *At*PDF1A; see Figs. 1 and 4) was observed without affecting the original hydrogen-bonding network, eventually leading to an additional bond in the closed state between the backbone N atom of Ile42 (corresponding to Val48 in *At*PDF1A) and the alkyl carbonyl chain of actinonin. In this respect, we revealed that the modification of this hydrophobic pocket stabilizes the enzyme–substrate complex in the transition state while making it highly reactive to perform the enzymatic hydrolysis reaction efficiently. In this work, we show that the glutamate which replaces the important leucine in motif 2 of human PDF1A (L112E in human-like PDF) is hydrogen-bonded both to the glutamine (Gln54 in human-like PDF1A) and the peptide (Figs. 5*a*, 5*b* and 5*c*), which strongly modifies the network of interactions in the oxyanion hole-like state. As a consequence, the transition state of the reaction is likely to be highly disturbed, with a probable effect on the reaction rate. Accordingly, kinetic experiments have already shown that the L112E substitution of *A. thaliana* PDF1A reduces the k_{cat} value by three orders of magnitude (Table 2). In contrast, the reverse mutation in human enzyme (E115L) has no effect, but the double substitution C50G/E115L increases the reaction rate by three orders of magnitude (Table 2). These data highlight the important contribution of the cysteine which replaces the glycine at position 50 and most likely reduces the flexibility of the enzyme around the ligand in the human PDF.

Hence, we show in this work that the two mutated residues in the active site of the human-like PDF affect the stability of the protein and decrease the affinity for the substrate by reducing the ligand-binding site volume. In addition, by creating new interactions with catalytic residues and substrate, the two mutated residues in human-like PDF strongly modify the transition state of the reaction, which leads to a reduced overall reaction rate. Our work suggests that the evolutionary double substitution G50C/L115E found in human PDF strongly disturbs the molecular events accounting for the deformylation reaction catalyzed by this enzyme, making it less efficient than any other prokaryotic PDF.

5. Concluding remarks

How can we explain the evolutionary selection of a different deformylation reaction speed of mammalian PDFs from the plant counterpart PDF1A or other prokaryotic PDFs? It has previously been suggested that because of their low activity and the lack of physiological evidence for *in vivo* activity mammalian PDFs have no cellular function (Nguyen *et al.*, 2003). Nevertheless, this hypothesis proved to be unconvincing as it was subsequently shown that mammalian mitochondrial PDFs are essential enzymes and that inhibition of the deformylase activity promotes cell death or proliferation arrest in a wide variety of cell lines, including cancer cells (Boularot *et al.*, 2007; Escobar-Alvarez *et al.*, 2010; Lee *et al.*, 2004). It has also been shown that the associated catalytic efficiency is much higher than expected from some studies (Serero *et al.*, 2003). Moreover, it has been shown that inhibition of human PDF downgrades the accumulation of mito-chondrially encoded proteins, respiratory complex assembly and the ATP level (Escobar-Alvarez *et al.*, 2010). Previous proteomic analysis of the 13 bovine mitochondrially encoded proteins revealed that only the Cox III subunit of cytochrome oxidase undergoes the N-terminal methionine excision (NME) process (Walker *et al.*, 2009), although seven of the 13 proteins were clearly predicted to undergo a systematic NME process (Giglione *et al.*, 2004). Whatever occurs, the NME process occurring in vertebrate mitochondria appears to differ from those observed in plant mitochondria, chloroplasts and bacteria because in this case the formyl moiety is removed from at least 94% of a larger organellar-encoded proteome (more than 5000 proteins in bacteria and >57 in organelles with a large genome such as plants and other non-animal organisms). As mammalian PDFs act on a reduced number of substrates, one could surmise that the double substitution conserved in vertebrate PDFs, even if it does not provide functional benefits, is maintained because its reduced activity is sufficient to ensure the NME process of a few crucial proteins. This effect could be also compensated by an increase of the amount of PDF synthesized, with or without a better binding capacity of the protein to the ribosome (Giglione *et al.*, 2009). Finally, we could also not exclude that the emergence of this new type of PDFs prevents noncognate reactions occurring in the peculiar environment of the mitochondrion.

References

Amero, C. D., Byerly, D. W., McElroy, C. A., Simmons, A. & Foster, M. P. (2009). *Biochemistry*, **48**, 7595–7607.
Ashkenazy, H., Erez, E., Martz, E., Pupko, T. & Ben-Tal, N. (2010). *Nucleic Acids Res.* **38**, W529–W533.
Becker, A., Schlichting, I., Kabsch, W., Groche, D., Schultz, S. & Wagner, A. F. (1998). *Nature Struct. Biol.* **5**, 1053–1058.

research papers

Becker, A., Schlichting, I., Kabsch, W., Schultz, S. & Wagner, A. F. (1998). *J. Biol. Chem.* **273**, 11413–11416.

Berg, A. K. & Srivastava, D. K. (2009). *Biochemistry*, **48**, 1584–1594.

Boularot, A., Giglione, C., Artaud, I. & Meinnel, T. (2004). *Curr. Opin. Investig. Drugs*, **5**, 809–822.

Boularot, A., Giglione, C., Petit, S., Duroc, Y., Alves de Sousa, R., Larue, V., Cresteil, T., Dardel, F., Artaud, I. & Meinnel, T. (2007). *J. Med. Chem.* **50**, 10–20.

Bowie, J. U., Reidhaar-Olson, J. F., Lim, W. A. & Sauer, R. T. (1990). *Science*, **247**, 1306–1310.

Brünger, A. T., Adams, P. D., Clore, G. M., DeLano, W. L., Gros, P., Grosse-Kunstleve, R. W., Jiang, J.-S., Kuszewski, J., Nilges, M., Pannu, N. S., Read, R. J., Rice, L. M., Simonson, T. & Warren, G. L. (1998). *Acta Cryst.* D**54**, 905–921.

Chen, D. Z., Patel, D. V., Hackbarth, C. J., Wang, W., Dreyer, G., Young, D. C., Margolis, P. S., Wu, C., Ni, Z.-J., Trias, J., White, R. J. & Yuan, Z. (2000). *Biochemistry*, **39**, 1256–1262.

Chen, M., Choi, Y., Voytas, D. F. & Rodermel, S. (2000). *Plant J.* **22**, 303–313.

Clements, J. M., Beckett, R. P., Brown, A., Catlin, G., Lobell, M., Palan, S., Thomas, W., Whittaker, M., Wood, S., Salama, S., Baker, P. J., Rodgers, H. F., Barynin, V., Rice, D. W. & Hunter, M. G. (2001). *Antimicrob. Agents Chemother.* **45**, 563–570.

Dardel, F., Ragusa, S., Lazennec, C., Blanquet, S. & Meinnel, T. (1998). *J. Mol. Biol.* **280**, 501–513.

DeLano, W. L. (2002). *PyMOL.* http://www.pymol.org.

Dirk, L. M., Williams, M. A. & Houtz, R. L. (2001). *Plant Physiol.* **127**, 97–107.

Dirk, L. M., Williams, M. A. & Houtz, R. L. (2002). *Arch. Biochem. Biophys.* **406**, 135–141.

Escobar-Alvarez, S., Gardner, J., Sheth, A., Manfredi, G., Yang, G., Ouerfelli, O., Heaney, M. L. & Scheinberg, D. A. (2010). *Mol. Cell. Biol.* **30**, 5099–5109.

Escobar-Alvarez, S., Goldgur, Y., Yang, G., Ouerfelli, O., Li, Y. & Scheinberg, D. A. (2009). *J. Mol. Biol.* **387**, 1211–1228.

Fieulaine, S., Boularot, A., Artaud, I., Desmadril, M., Dardel, F., Meinnel, T. & Giglione, C. (2011). *PLoS Biol.* **9**, e1001066.

Fieulaine, S., Juillan-Binard, C., Serero, A., Dardel, F., Giglione, C., Meinnel, T. & Ferrer, J.-L. (2005). *J. Biol. Chem.* **280**, 42315–42324.

Fourmy, D., Meinnel, T., Mechulam, Y. & Blanquet, S. (1993). *J. Mol. Biol.* **231**, 1068–1077.

Giglione, C., Boularot, A. & Meinnel, T. (2004). *Cell. Mol. Life Sci.* **61**, 1455–1474.

Giglione, C., Fieulaine, S. & Meinnel, T. (2009). *Trends Biochem. Sci.* **34**, 417–426.

Giglione, C., Serero, A., Pierre, M., Boisson, B. & Meinnel, T. (2000). *EMBO J.* **19**, 5916–5929.

Giglione, C., Vallon, O. & Meinnel, T. (2003). *EMBO J.* **22**, 13–23.

Gouet, P., Courcelle, E., Stuart, D. I. & Métoz, F. (1999). *Bioinformatics*, **15**, 305–308.

Kabsch, W. (2010). *Acta Cryst.* D**66**, 125–132.

Landau, M., Mayrose, I., Rosenberg, Y., Glaser, F., Martz, E., Pupko, T. & Ben-Tal, N. (2005). *Nucleic Acids Res.* **33**, W299–W302.

Laskowski, R. A., MacArthur, M. W., Moss, D. S. & Thornton, J. M. (1993). *J. Appl. Cryst.* **26**, 283–291.

Lee, M. D., Antczak, C., Li, Y., Sirotnak, F. M., Bornmann, W. G. & Scheinberg, D. A. (2003). *Biochem. Biophys. Res. Commun.* **312**, 309–315.

Lee, M. D., She, Y., Soskis, M. J., Borella, C. P., Gardner, J. R., Hayes, P. A., Dy, B. M., Heaney, M. L., Philips, M. R., Bornmann, W. G., Sirotnak, F. M. & Scheinberg, D. A. (2004). *J. Clin. Invest.* **114**, 1107–1116.

Li, Y., Chen, Z. & Gong, W. (2002). *Biochem. Biophys. Res. Commun.* **295**, 884–889.

McCoy, A. J., Grosse-Kunstleve, R. W., Storoni, L. C. & Read, R. J. (2005). *Acta Cryst.* D**61**, 458–464.

Meinnel, T. (2000). *Parasitol. Today*, **16**, 165–168.

Meinnel, T. & Giglione, C. (2008). *Proteomics*, **8**, 626–649.

Meinnel, T., Lazennec, C. & Blanquet, S. (1995). *J. Mol. Biol.* **254**, 175–183.

Meinnel, T., Lazennec, C., Dardel, F., Schmitter, J.-M. & Blanquet, S. (1996). *FEBS Lett.* **385**, 91–95.

Meinnel, T., Lazennec, C., Villoing, S. & Blanquet, S. (1997). *J. Mol. Biol.* **267**, 749–761.

Murshudov, G. N., Skubák, P., Lebedev, A. A., Pannu, N. S., Steiner, R. A., Nicholls, R. A., Winn, M. D., Long, F. & Vagin, A. A. (2011). *Acta Cryst.* D**67**, 355–367.

Narayanan, S. S., Sokkar, P., Ramachandran, M. & Nampoothiri, K. M. (2011). *FEMS Microbiol. Lett.* **320**, 40–47.

Nguyen, K. T., Hu, X., Colton, C., Chakrabarti, R., Zhu, M. X. & Pei, D. (2003). *Biochemistry*, **42**, 9952–9958.

Ragusa, S., Mouchet, P., Lazennec, C., Dive, V. & Meinnel, T. (1999). *J. Mol. Biol.* **289**, 1445–1457.

Ross, S., Giglione, C., Pierre, M., Espagne, C. & Meinnel, T. (2005). *Plant Physiol.* **137**, 623–637.

Roussel, A. & Cambillau, C. (1989). *Silicon Graphics Geometry Partners Directory*, pp. 77–78. Silicon Graphics, Mountain View, California, USA.

Schmitt, E., Guillon, J. M., Meinnel, T., Mechulam, Y., Dardel, F. & Blanquet, S. (1996). *Biochimie*, **78**, 543–554.

Schmitt, E., Meinnel, T., Panvert, M., Mechulam, Y. & Blanquet, S. (1993). *J. Mol. Biol.* **233**, 615–628.

Serero, A., Giglione, C. & Meinnel, T. (2001). *J. Mol. Biol.* **314**, 695–708.

Serero, A., Giglione, C., Sardini, A., Martinez-Sanz, J. & Meinnel, T. (2003). *J. Biol. Chem.* **278**, 52953–52963.

Sharon, I., Battchikova, N., Aro, E.-M., Giglione, C., Meinnel, T., Glaser, F., Pinter, R. Y., Breitbart, M., Rohwer, F. & Béjà, O. (2011). *ISME J.* **5**, 1178–1190.

Van Aller, G. S., Nandigama, R., Petit, C. M., DeWolf, W. E. Jr, Quinn, C. J., Aubart, K. M., Zalacain, M., Christensen, S. B., Copeland, R. A. & Lai, Z. (2005). *Biochemistry*, **44**, 253–260.

Walker, J. E., Carroll, J., Altman, M. C. & Fearnley, I. M. (2009). *Methods Enzymol.* **456**, 111–131.

Zhou, Z., Song, X. & Gong, W. (2005). *J. Biol. Chem.* **280**, 42391–42396.

Zhou, Z., Song, X., Li, Y. & Gong, W. (2004). *J. Mol. Biol.* **339**, 207–215.